Applied Surface Science 561 (2021) 149959

Contents lists available at ScienceDirect

Applied Surface Science

journal homepage: www.elsevier.com/locate/apsusc

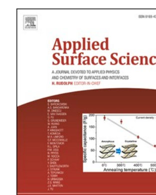

Full Length Article

Computational modeling of electrolytic deposition of a single-layer silicon film on silver and graphite substrates

Ksenia A. Ivanichkina [a,b,*], Alexander Y. Galashev [a,b], Andrey V. Isakov [a]

[a] *Institute of High-Temperature Electrochemistry, Ural Branch, Russian Academy of Sciences, Academic Str. 20, Yekaterinburg 620990, Russia*
[b] *Ural Federal University named after the first President of Russia B.N. Yeltsin, Mira Str., 19, Yekaterinburg 620002, Russia*

ARTICLE INFO

Keywords:
Molten salts
Molecular dynamics
Surface diffusion
Silicon films
Substrate

ABSTRACT

Electrodeposition of silicon from a KF-KCl-KI salt melt at 1000 K using silver and graphite substrates has been studied by the molecular dynamics method. Silicon films of monatomic thickness with a predominantly hexagonal honeycomb structure were obtained on each substrate. The adhesion energy between the obtained film and the silver substrate is 2.5 times higher than that between the film and the graphite substrate. A single cluster grows much faster on a graphite substrate than on a silver substrate, where several clusters are formed at once. As the substrates are filled with silicon, the diffusion coefficient of Si atoms decreases faster on a graphite substrate than on a silver one. The silver substrate is completely covered with silicon, while a three-dimensional Si cluster begins to grow on a graphite substrate incompletely filled with silicon. The obtained silicon films on both substrates do not have the characteristic buckling, which is found in silicene prepared by the chemical vapor deposition on a silver substrate. Films obtained on both substrates have low mechanical stress. The stress distribution in the case of a graphite substrate is more uniform.

1. Introduction

Solar energy dominates among renewable energy sources because it has a huge potential due to availability and variety of possible applications in different fields. The main problem to increase the power of the solar battery is obtaining materials for highly efficient solar cell creations. Nowadays, high-purity silicon is the most promising material for solar cells, and a path of its cost reduction should be thoroughly studied.

At the present time, silicon wafers fabrication is one of the most expensive operations. Obtaining solar silicon requires a lot of energy due to the high crystallization temperature of silicon and the complex processing of this material [1]. However, pure silicon can be obtained at low temperatures in liquid molten salts [2,3]. Fluoride melts were found to be a sufficiently successful environment for pure silicon production; however, such melts are quite aggressive, although they have the lowest liquidus temperature [4]. The electronegativity and oxidizing properties of halogens decrease as their atomic mass increases. In terms of reaction, the activity of iodine is lower than that of all other halogens, and even more so for fluorine. The use of iodides reduces the reactivity during high-temperature exchange reactions. The atomic radius of fluorine R_F is 3.78 times larger than the radius of the Si atom, while the radii of the I and Si atoms are comparable ($R_I / R_{Si} = 1.03$). The closeness of the I and Si radii can facilitate the formation of a perfect crystal structure of Si films during the electrodeposition. It is supposed that the electrolytic deposition from the KF-KCl-KI ternary melt makes it possible not only to obtain high-purity silicon [5], but also to achieve a uniform distribution of the dopant (p- or n-type) using the coprecipitation method [6]. The initial concentration of Si in the melt is given by the K_2SiF_6 addition.

The electrodeposition process is accompanied both by electrochemical and by chemical reactions. Moreover, chemical reactions are usually initiated using the transfer of electrons. At the final stage of electrodeposition, the unbound ions of the depositing substance, which are reduced at the cathode, are present in the melt. Thus, a coating is created using an electric current. It is the final stage of electrodeposition that is considered in this work.

The formation of coatings by electrolytic deposition from molten salts is a promising method for the synthesis of new materials. Such factors as relatively low electrolysis temperatures, the possibility to obtain coatings in the oxygen-free melt environment and to vary the coating composition and properties depending on the melt composition

* Corresponding author at: Institute of High-Temperature Electrochemistry, Ural Branch, Russian Academy of Sciences, Academic Str. 20, Yekaterinburg 620990, Russia.

E-mail address: ivanichkina@ihte.uran.ru (K.A. Ivanichkina).

https://doi.org/10.1016/j.apsusc.2021.149959
Received 18 February 2021; Received in revised form 19 April 2021; Accepted 26 April 2021
Available online 4 May 2021
0169-4332/© 2021 Elsevier B.V. All rights reserved.

and the substrate orientation attract global interest to the electrochemical deposition method [7]. In this regard, it is important to understand the initial stage of the coating formation by the electrolytic deposition from the melt.

The molecular dynamics (MD) method is one of the most accurate predictive computer methods. In the classical version of this method (using empirical or model interaction potentials), a large set of physicochemical properties (thermodynamic, kinetic, and structural) can be obtained in one calculation. With the coordinates of the atoms at each moment of time, the structure of the simulated object can be investigated in different ways in the MD model. The radial distribution function $g(r)$ is a traditionally used characteristic to represent the structure of liquids and solids. The function $g(r)$ reflects the average distribution of atoms around any given atom in the system. This is a one-dimensional function and it describes the structure in an averaged form. The three-dimensional structure in the model can be analyzed by the method of statistical geometry, based on the construction of Voronoi polyhedral [8]. Moreover, MD calculations make it possible to determine the diffusion coefficients of the melt components [9], thermal conductivity and surface tension of the melt [10,11].

Nowadays, there is a global problem in obtaining silicon films of the monoatomic thickness (silicene). So far, the preparation of silicene has been carried out by the method of deposition from the ultra-high vacuum, mainly on silver substrates of various orientations: (1 1 1), (1 0 0), (1 1 0) [12,13]. These results can be explained by the presence of p-d hybridization between Ag-Si atoms, which leads to the stabilization of silicene grown on the silver substrate. Schneider et al. [14] studied the structures formed by silicon on pyrolytic graphite by the magnetron sputtering method. The images obtained using scanning tunneling microscopy (STM) speak in favor of the nanoclusters and silicon nanoribbons formation of various orientations. Feng et al. [15] obtained silicon films on the Ag(1 1 1) substrate. At high temperatures (above 450 K) the silicon coatings on the Ag(1 1 1) substrate tend to form a highly ordered honeycomb structure.

In the present work the initial growth stages of a silicon film deposited from the KF-KCl-KI melt on Ag(0 0 1) and graphite substrates are simulated by the MD method. The difference in the substrate material nature can have a significant influence on the resulting coating structure imperfections, due to the varying adhesion of Si-atoms to the substrate.

The purpose of this work is to create a model, which reflects the first stages of the new phase (clusters) nucleation in the molten electrolyte, and to apply this model to the study of the mechanism of the coating formation. The rate of the continuous coating formation depends on the surface mobility of Si-clusters and adhesion between silicon and substrate.

2. Computational method

2.1. System formation

At the first stage, the system was formed by three crystals (KCl, KF, KI with fcc lattice) located over the Ag(0 0 1) or graphite surfaces. The crystals were located at the distance of ≈0.4 nm from each other and from the substrate. The total number of particles in the system with a silver substrate (system I) was 12,359, in the system with a graphite substrate (system II) 19,312 atoms were used. The content of the elements forming the melt was the same for both systems: 1,728 KF atoms (19.2 mol%), 864 KCl atoms (9.6 mol%), 6,400 KI atoms (71.2 mol%).

The silver substrate, oriented to the melt by the (0 0 1) plane, contained 3,423 atoms located in 5 layers of a face centered lattice. The graphite substrate was formed by 10,320C atoms and consisted of 4 graphene sheets, the upper one of which was in contact with the molten salt. Flat hexagonal lattices characteristic of graphene were arranged in a checkerboard pattern according to the ABAB scheme with a distance between them of 0.335 nm. The atoms of both substrates participated in thermal motion. The interaction of atoms in the substrate was described by the EAM potential (in the case of the Ag(0 0 1) substrate) [16], and by the Tersoff potential (in the case of the graphite substrate) [17]. These potential functions and their parameters are listed in Appendix A.

The interaction in salts and salt mix was described by the hybrid potential consisting of the Lennard-Jones term and the Coulomb one. The Lennard-Jones (LJ) potential function with the Coulomb term is given by:

$$\text{Đ¤}(r_{ij}) = \frac{Z_i Z_j}{r_{ij}} + 4\varepsilon\left[\left(\frac{\sigma}{r_{ij}}\right)^{12} - \left(\frac{\sigma}{r_{ij}}\right)^{6}\right] \quad (1)$$

where Z_i is the charge of the i-atom, $r_{ij} = |r_i - r_j|$ is the distance between atoms i and j, ε is the depth of the potential well, σ is the distance at

Table 1
Lennard-Jones potential parameters for describing interaction in the melt.

ion pair i-j	ε (eV)	σ (Å)
K-K	0.0323	4.886
F-F	0.00781	3.12
Cl-Cl	0.00509	4.417
I-I	0.0147	4.009
K-Cl	0.0128	4.6514
K-F	0.0159	4.0029
K-I	0.0218	4.447
F-Cl	0.00631	3.769
F-I	0.0107	3.565
Cl-I	0.00865	4.213
Si-K	0.0253	3.216
Si-F	0.00198	3.9515
Si-I	0.0109	3.876
Si-Cl	0.0124	3.995

Table 2
Morse potential parameters for describing interaction on the substrate surface.

ion pair i-j	D^o_{ij} (eV)	α_{ij} (Å^{-1})	r^o_{ij} (Å)
Si-Ag	0.09	1.115	3.450
Si-C	0.435	4.648	1.947

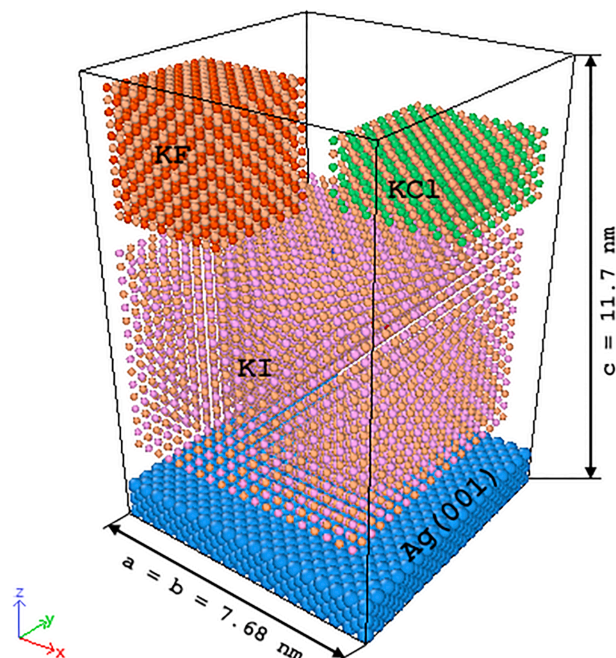

Fig. 1. General view of the original system at time t = 0 ns. The system dimensions are shown in the figure.

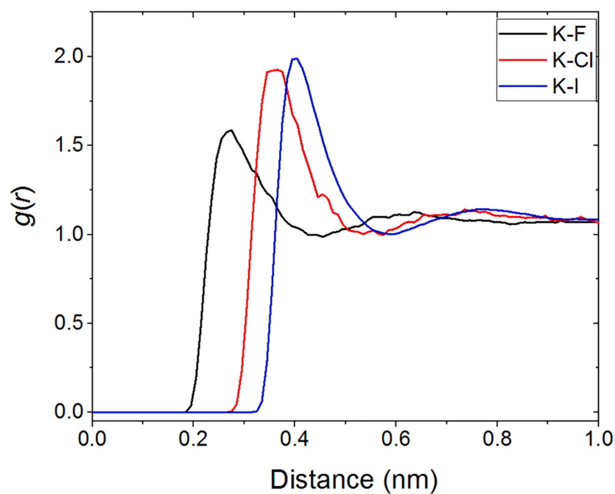

Fig. 2. Radial distribution functions of the "cation-anion" systems: K-F (black line); K-Cl (red line); K-I (blue line) after the melting process. (For interpretation of the references to colour in this figure legend, the reader is referred to the web version of this article.)

which the interaction between the *i* and *j* atoms becomes zero. Charges of the system components are: $Z_K = +1$, $Z_{Cl} = -1$, $Z_F = -1$, $Z_I = -1$, $Z_{Si} = +4$. The substrates were the zero charge.

Parameters of the Lennard-Jones potential presented in Table 1. The K-K, F-F-, Cl-Cl, I-I parameters were taken from [18–20].

The Lennard-Jones potential is not universal and poorly describes solid–solid interactions. LJ systems do not reproduce such physical characteristics as thermal conductivity and elastic properties [21]. Therefore, in the present model, the interaction of silicon with substrate surfaces was described by the Morse pair potential [22]:

$$Ð¤(r_{ij}) = D^{o}_{ij}\left[\exp\left\{-2\alpha_{ij}(r_{ij}-r^{o}_{ij})\right\} - 2\exp\left\{-\alpha_{ij}(r_{ij}-r^{o}_{ij})\right\}\right] \quad (2)$$

where D_o is the depth of the potential well, α is the parameter that determines the "rigidity" of the bond, r_o is the equilibrium bond length. The Morse potential parameters are given in Table 2. The Si-C, Si-Ag Morse parameters were taken from [23] and [24], respectively.

When the static system was formed, the MD modeling stage began.

2.2. Melting and relaxation of the system

The system described in the previous paragraph was melted. The melting process details are discussed below. The periodic boundary conditions acted in the (*x*,*y*) directions and rigid walls of the MD box were used in the z-direction. Parameters of the simulation cell are shown in Fig. 1. The integration step of the motion equations was 1 fs. In order to avoid the rapid heating of the system, a geometric optimization was performed first. During the geometric optimization the structural relaxation of the system was carried out. The minimization procedure was performed by the Polak-Ribier conjugate gradient method [25] to find the potential minimum of the system, i.e. the difference in potential energy at the previous and current steps was calculated; this difference was assumed not to exceed 10^{-5} eV. Further, under NVT ensemble conditions, the system was heated to 300 K for 0.1 ns. For the next 1.4 ns, the system was heated stepwise to 1750 K with the temperature step of 50 K. On the following stage, the relaxation of this system in the NPT ensemble was performed. The required density of the melt ($\rho \approx 1.9$ g / cm^3) was achieved during 0.5 ns. Analysis of the radial distribution function $g(r)$ was performed to confirm the transition of all system components to a liquid state. Fig. 2 demonstrates that all melt components at the last stage of the melting process (after 1.9 ns) are liquid.

The random choice of starting points for the Si^{4+} ion determines the

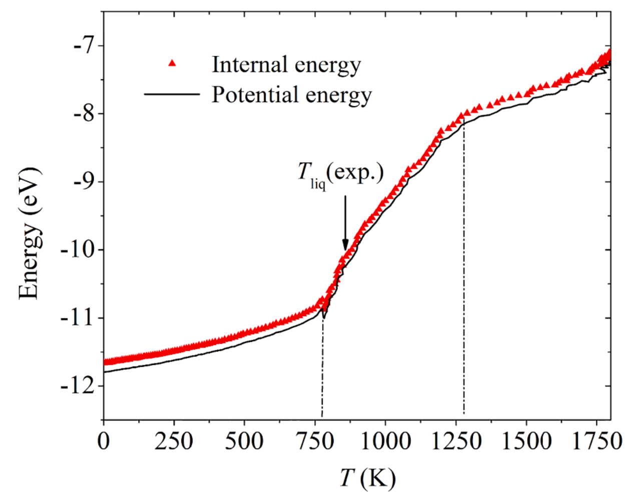

Fig. 3. Changes in the internal energy of the KF-KCl-KI melt during heating from 200 K to 1750 K.

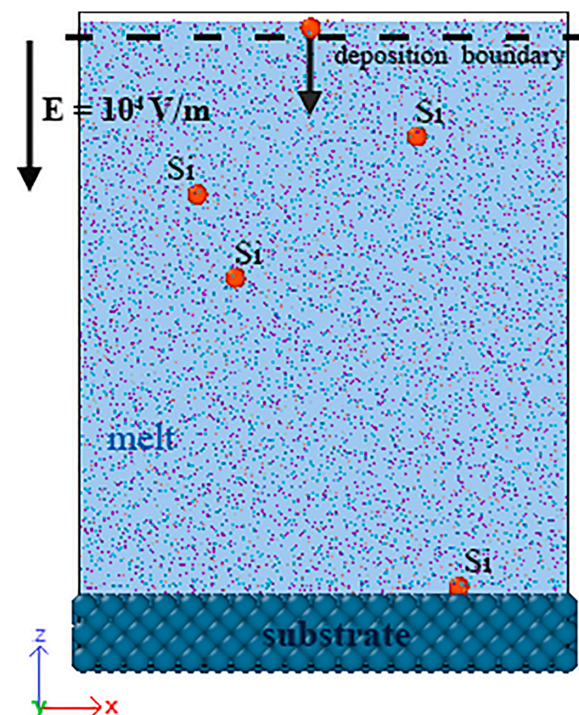

Fig. 4. Schematic representation of the Si^{4+} deposition process from the melt to the substrate. Silicon ions were introduced in the system periodically, crossing the deposition boundary (indicated by the dash-dotted line), the particles moved through the melt in the substrate direction under the action of the electrical field E.

statistical nature of this study. The ion was launched in the system every 30,000 time steps, which corresponds to a time of 30 ps. It was at such intervals that the coordinates of the system under study were recorded. This time noticeably exceeds the time, which is necessary for the ion to occupy its site (usually from 1 to 10 ps) after reaching the substrate. Therefore, the time of 30 ps can be considered as the absolute error in determining the time of complete coverage of the substrate with silicon or other characteristic instants.

Fig. 3 illustrates the internal and potential *U* energy dependence of the (KF-KCl-KI) system on the temperature. The behaviors of both energies are almost identical. The arrow shows the experimental value (858 K) of the liquidus temperature [4]. The middle section of $U(T)$

function is distinguished by the rapid growth, which corresponds to the system phase transition. The phase transition range is highlighted by dash-dotted lines and corresponds to the temperature range of 750–1250 K. It should be noted that the liquidus temperature of a real salt system with a different concentration of components lies in the temperature range of 775–985 K [26].

2.3. Silicon particles deposition from the melt and adhesion energy

After the formation of the "melt - substrate" interface, silicon was introduced into the system. The superheated melt was cooled to the working temperature of 1000 K, it should be noted that the experimental temperature of the real electrolytic process ranges from 993 to 998 K and varies depending on the molar concentration of the components [27]. The silicon deposition process is shown in Fig. 4, and it is also presented in the Supplementary material. Charged Si^{4+} ions were periodically introduced through the deposition boundary of the MD cell (z = 11 nm). In this case, in the liquid electrolyte the electric field ($E = 10^4$ V/m) acted towards the substrate along the z-axis. The electric field imposition simulated the electrical driving force attended in the electrolytic process. The Si deposition process was in the NVT-ensemble.

Adhesion energy is an important characteristic of the film / substrate system. Thin films are often very brittle and exist only because of the substrates that support them. The energy of adhesion determines largely how well the substrate provides the film strength. In addition, the durability of thin-film devices used in electronic microcircuits also mainly depends on the degree of adhesion of the film to the substrate. In other words, the performance of thin films is dictated by the adhesive forces. For example, at poor adhesion the film wears out quickly. However, there are situations where strong adhesion interferes with the processing step, as in the case of peelable films. The calculated adhesion energy characterizes the adhesion force that occurs between the formed silicon film and the substrate due to the intermolecular van der Waals interaction. The E_{ad} values were calculated according to the formula:

$$E_{ad} = E_{Si} + E_{sub} - E_{tot} \quad (1)$$

E_{Si} is the internal energy of the silicon subsystem, E_{sub} is the internal energy of the pristine substrate, E_{tot} is the internal energy of the "Si-substrate" system.

Whereas the changes in the adhesion energy to the substrate can represent the materials coupling force and the new surface growth dynamics, the analysis of the time dependence of the studied subsystem internal energy can be useful for the identification of the cluster growth stages. This can be assumed from the fact that the internal energy of the subsystem (E_{int}) is the value of the specific interatomic potential interaction, which describes the subsystem under study.

2.4. Diffusion

The diffusion coefficient was calculated according to the formula:

$$D = \frac{1}{2\Gamma N}\lim_{t\to\infty}\frac{1}{t}\langle\sum_{i=1}^{N}(\Delta\mathbf{r}_i)^2\rangle \quad (2)$$

where for three-dimensional space $\Gamma = 3$, N is the number of particles in the system, t is the time of observation of the displacement of atoms at a certain initial time t_0, $\Delta\mathbf{r}_i(t) = \mathbf{r}_i(t) - \mathbf{r}_i(t_0)$ is the displacement of the i atom relative to the position that it occupied at the initial time instant t_0, summation is performed over all N particles of the system, $\langle\ldots\rangle$ denotes averaging over the initial times used to determine D.

The initial velocity of Si^{4+} ions was −0.01 nm/ps ("-" is the reflection of the velocity vector direction to the substrate). A new silicon ion was introduced into the system every 30 ps. The choice of such time interval for the introduction of Si ions into the salt melt was dictated by the following considerations. We will consider the diffusion as a spontaneous process of the matter transfer, leading to the equalization of concentrations and chemical potential as a result of the thermal motion of molecules, ions and particles. Using formula (2), we calculated the average (for systems with silver and graphite substrates) diffusion coefficient of Si^{4+} ions (~1.1×10^{-5} $cm^2\ s^{-1}$) in the volume of the electrolyte. The experimental value D of Si^{4+} ions in the KF – KCl – K_2SiF_6 system was determined to be 3.2×10^{-5} $cm^2\ s^{-1}$ at 923 K [28].

During the time of 30 ps, the Si^{4+} ion, as a rule, had time to pass through the melt and sink to the substrate surface. Then the ion diffused over the substrate surface until it found a proper site, i.e. the place where it was firmly attached to the substrate. The deposition was carried out until the substrate surface was completely tiled with a silicon layer.

2.5. Statistical geometry method

The method of statistical geometry is based on obtaining statistical distributions for elements of Voronoi polyhedra (VP) or modified polyhedral [29,30]. VP selects a Voronoi region in space, all points of which are closer to the given center i than to any other center of the system. All geometric neighbors can be divided into main (direct) and non-main ones. For the former, the midpoint of the segment connecting the geometric neighbor to the center i belongs to the VP face, and for the latter it does not. A polyhedron constructed including only direct neighbors is called a simplified polyhedron [31].

In order to evaluate the closeness of the structure of the silicon films obtained in the present study with the structure of silicene, we performed a statistical analysis of the structure based on the construction of Voronoi polyhedra. Due to the fact that neither silicene nor the deposited silicon films have an ideal flat shape, it is possible to construct three-dimensional Voronoi polyhedra. Due to the small size of the z-coordinate (the z axis is perpendicular to the plane of the substrate) of atoms, such polyhedrons will not have a high degree of symmetry. To take into account the effect of the substrate material, silicene, analogously to the silicon film obtained by us, was placed on the Ag(001) and graphite substrates. Molecular dynamics calculation of silicene on the corresponding substrates was carried out at the temperature of 300 K. The duration of the calculation was 1 million time steps. The shape of the polyhedra was estimated by the nonsphericity parameter [32]:

$$\eta = S^3/(36\pi V^2) \quad (3)$$

where S is the surface area of polyhedron and V is its volume.

In the cases where silicene was found on the Ag(001) and graphite substrates, close values of the parameter η were obtained: 2.64 and 2.63, respectively. These values are between the values of η for hexagonal ice (2.25) [33] and ideal tetrahedron (3.31). The VP nonsphericity for a silicon film deposited on the Ag(001) and graphite substrates turned out to be higher, it was 3.15 and 5.14, respectively.

In this study, we paid attention not only to the detailed structure of the obtained silicon films, but also to the degree of their stressed state. To determine the stress state of the films, we calculated the stress tensor for these thin layers. The entire film was divided into L strips. The film surface was subdivided both in the direction of the $0x$ axis and in the direction of the 0y axis. The calculation of the $\sigma_{\gamma\alpha}(l)$ stress appearing on the elementary area with the number l was determined by dividing the resulting force by its area S_l. The resulting force was determined as the sum of the vectors of all interatomic forces passing through the area [34]. When determining the $\sigma_{\gamma\alpha}(l)$ value, the interaction was taken into account both between solely film atoms and between the film and substrate atoms. Index γ shows the direction of the area orientation, and the index α (= x, y, z) indicates the direction of action of the resulting force component. Thus, the stress at an elementary area can be calculated according to the expression

$$\sigma_{\gamma\alpha}(l) = \langle\sum_i^n \frac{1}{\Omega}\left(mv_\gamma^i v_\alpha^i\right)\rangle + \frac{1}{S_l}\langle\sum_i^n \sum_{j\neq i}^{(u_i\leq u,u_j\geq u)}\left(f_{ij}^\alpha\right)\rangle, \quad (4)$$

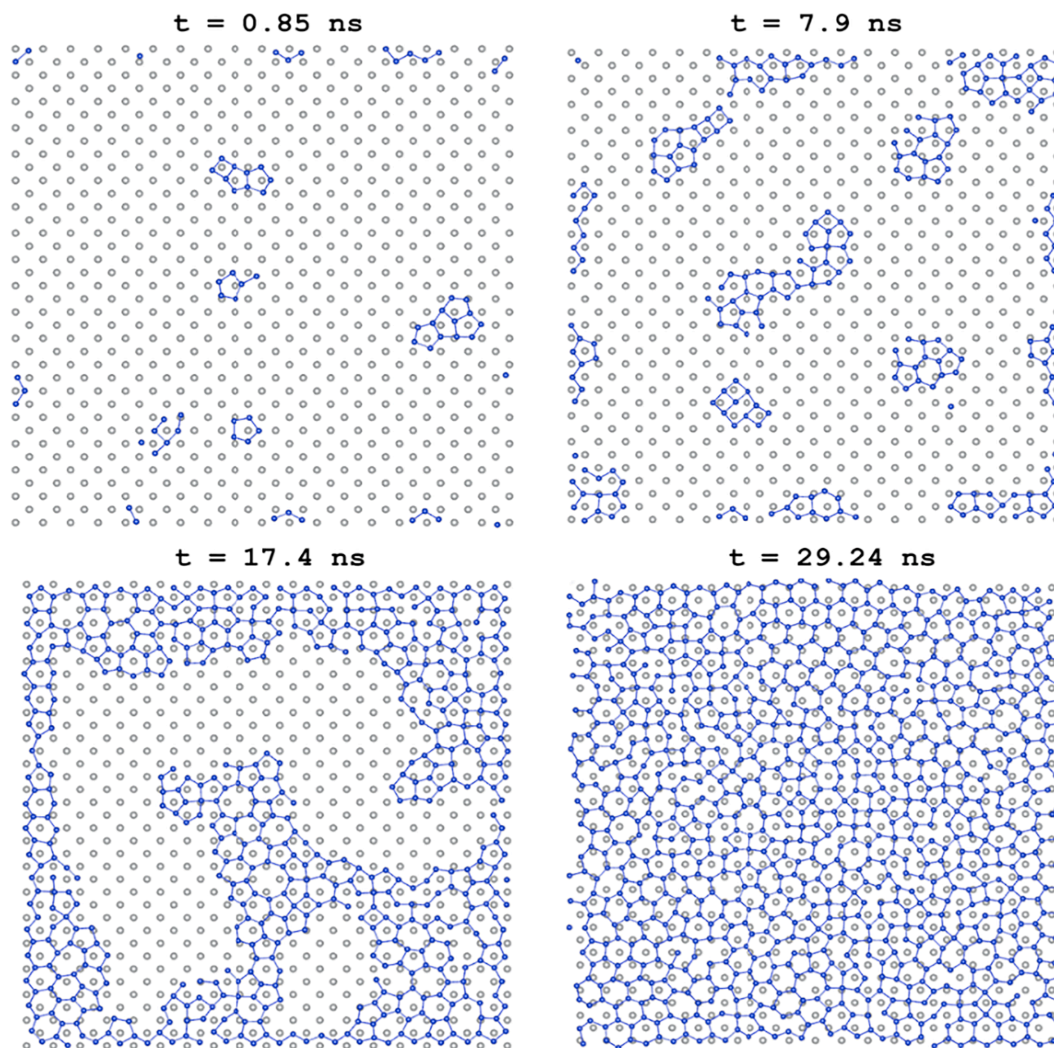

Fig. 5. Stages of two-dimensional silicon film growth on the silver substrate from the KF-KCl-KI melt (Si atoms are marked in blue). (For interpretation of the references to colour in this figure legend, the reader is referred to the web version of this article.)

where n is the number of atoms on the l area, m is the atomic mass, v_{α}^{i} is the α projection of the velocity of the i atom, Ω is the volume per atom, f_{ij}^{α} is the α projection of the resulting force from the interaction between i and j atoms that passes though the l area, and u_i is the coordinate of the atom i; the coordinate of the contact point of the straight line passing through the centers of the atoms i and j and the l surface element is denoted through the symbol u.

3. Results

The growth mechanism of a silicon film is highly dependent on the type of substrate on which the film is produced. The stages of silicon film growth on the Ag(0 0 1) and graphite substrates are shown in Figs. 5 and 6, respectively. The first image (Fig. 5) illustrates the initial stage of the stable Si-cluster formation. It can be noted that the embryonic structure of the silicon film appears (0.85 ns) even when a cluster containing only 13 atoms appears on the substrate. Small clusters form at different places of the surface. However, the locations of these clusters do not remain constant over time. We see that by the time of 7.9 ns the clusters have not only increased in size, but also changed their location. At this point in time, one can already observe the coalescence of clusters. Thus, starting from this moment, the growth of a silicon film on the Ag(0 0 1) substrate occurs not only due to an increase in the size of individual clusters, but also through their merging. It can be seen that by the time of 17.40 ± 0.03 ns the silicon film almost completely covered the substrate, except for two regions of unequal size. One of the silicon-free regions is large and it occupies most of the central region of the substrate. The smaller free area is near the bottom edge of the substrate. Further growth of the film occurs by compression of free cavities on the substrate, i.e. the growth proceeds from the boundaries of the cavities in their center. By the time of 22.24 ± 0.03 ns, the Ag(0 0 1) substrate was completely covered with a silicon film. Thus, the strong interaction of Si^{4+} ions with the Ag(0 0 1) substrate creates conditions for the growth of several silicon clusters at once, the coalescence of which makes it possible to cover most of the substrate. After the formation of Si-free cavities on the substrate, due to the low value of the adsorption energy for the boundaries of the cavities, new Si atoms are first added to them. Ultimately, the entire surface of the Ag(0 0 1) substrate is covered with a silicon film.

It can be emphasized that upon deposition on the silver substrate, the silicon film is formed mainly from six and five-link rings and appears as a uniform coating. Theoretical studies aimed at a detailed investigation of the interaction mechanisms between silicene (i.e. single layer silicon) and metal atoms confirm the obtained results on the determination of the most energetically favorable positions of the Si-atoms [35].

In the case of the graphite substrate, the single Si-cluster is formed, it increases gradually, and eventually covers the entire substrate surface (Fig. 6). The initial stable Si-cluster on the graphite substrate is formed

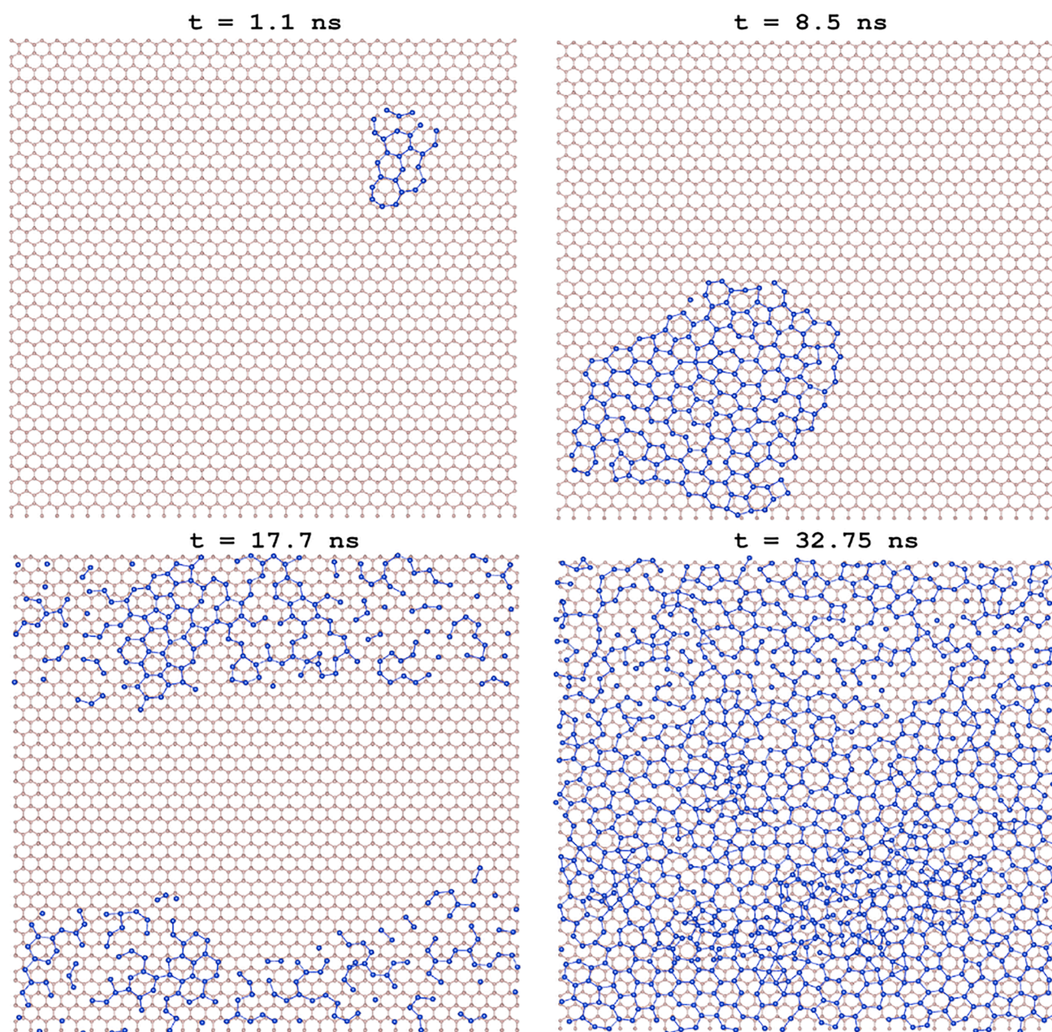

Fig. 6. Stages of two-dimensional silicon film growth on the graphite substrate from the KF-KCl-KI melt (Si atoms are marked in blue). (For interpretation of the references to colour in this figure legend, the reader is referred to the web version of this article.)

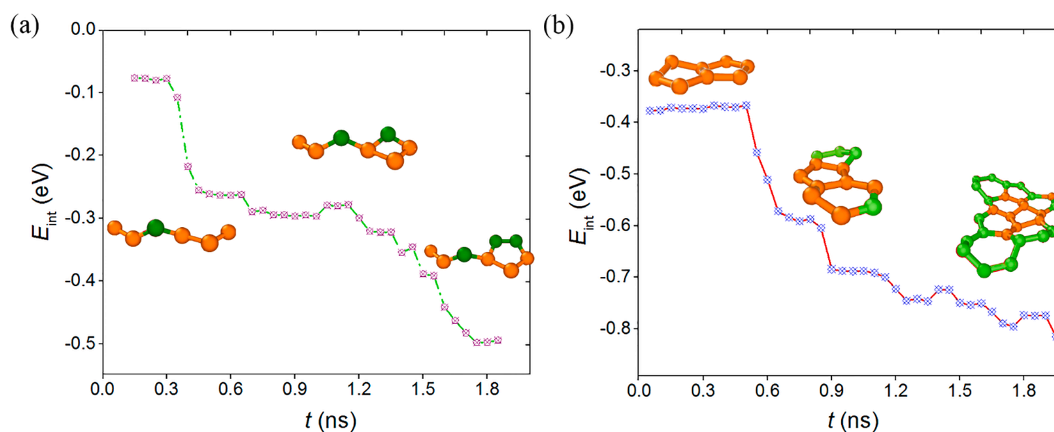

Fig. 7. Time dependence of the Si-clusters internal energy changes at different stages of the cluster formation: (a) system on the Ag(001) substrate, (b) system on the graphite substrate.

during 1.1 ns by 27Si-atoms. By the time of ~ 8.5 ns, the Si cluster on the substrate surface reaches a size covering up to 1/5 of the substrate surface area. However, such cluster turns out to be unstable, and by the time of 17.70 ± 0.03 ns it decays into two narrow bands occupying the upper and lower parts of the substrate surface. Subsequently, as the Si atoms are deposited, the bands begin to grow towards each other, forming a continuous silicon film on the substrate surface.

The hexagonal honeycomb structure of graphene sheets, which form a graphite substrate, initiates the formation of a local hexagonal packing of Si atoms at the substrate surface. However, the hexagonal

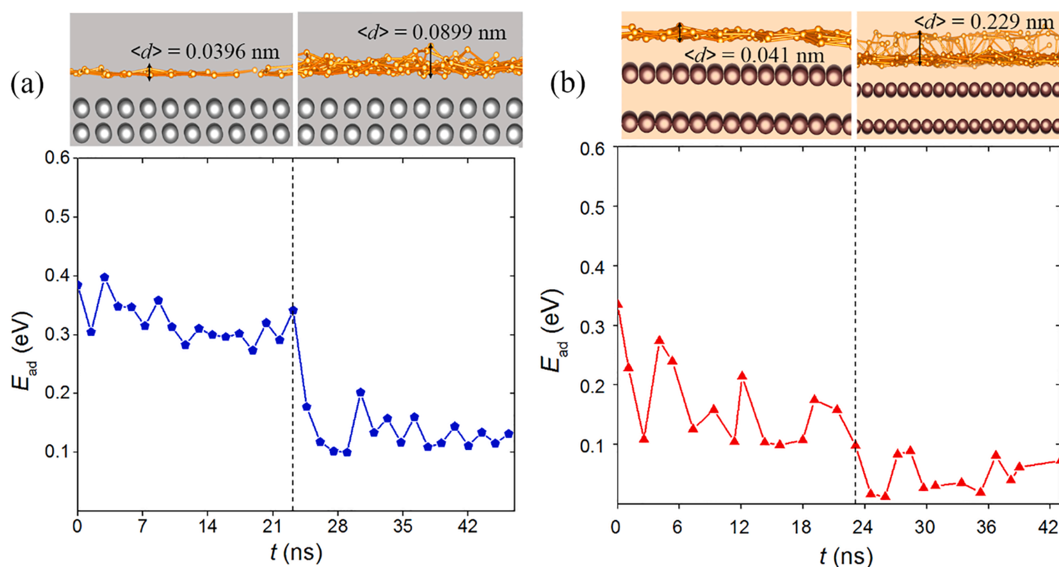

Fig. 8. Changes in the adhesion energy of Si/Ag (a) and Si/C (b) during the deposition of silicon. The dash-dotted line separates the stages of Si film growth: left field shows the process that takes place on the substrates when Si is present in the form of individual clusters; right field represents the stage of continuous film formation.

arrangement of Si atoms at the substrate surface has a local character. Probably, this is due to the mismatch of the lattice periods of graphene and silicene. The silicon film formed on graphite has a block structure. Moreover, the blocks formed from hexagonal Si-cells have different orientations. Linear structural defects are formed at the block boundaries. When the Si film covers most of the surface area of the substrate, the Si^{4+} ions tend to bind to the formed Si layer rather than to continue deposition on the substrate.

Fig. 7 illustrates the dependence of the internal energy changes in the Si-subsystem $E_{int}(t)$ for a silicon film on the Ag(001) substrate. It can be seen that the internal energy decreases stepwise, each step reflects the attachment of a new Si atom (green in the inset) to the stable cluster located at the substrate surface (orange in the inset). Liu et al. [36] performed an ab initio calculation by the molecular dynamics method of the formation energy of silicon clusters in the absence of a substrate and on an Ag(111) substrate. For a free-standing Si_6 cluster and the analogous cluster on the Ag(111) substrate, the values of formation energy were equal to −0.88 and −0.5 eV, respectively. The energy value E_{int} (-0.2 eV) determined from the first step in Fig. 7 can be considered as the energy of formation of a diatomic silicon cluster. The addition of each new Si atom to the cluster is accompanied by a decrease in the energy E_{int}. The energies of formation of five and six-link clusters on the Ag (001) substrate are ≈ -(0.47 – 0.50) eV. These energies are less in absolute value than the corresponding energies obtained from ab initio calculations. The Si-rings formed in the model do not have any minimum energy, since they are influenced by the surrounding molten salt at high temperatures. In addition to the high mobility of the components in the melt, the formation of energetically more favorable Si-structures on the substrate is influenced by the interaction between Si atoms and the substrate.

Si clusters formed on the graphite substrate have lower internal energies than similar clusters formed on the Ag(001) substrate. The specific growth mechanism of a silicon film on the graphite surface was expressed in the initial formation of a small (of 27Si atoms) cluster, its growth, division into two parts, followed by filling the free space of the substrate with silicon. However, before a continuous film of silicon is formed, locally buildups (layers) of Si atoms appear. The inserts in Fig. 7b show the above-described structural changes during the formation of the Si film on graphite. Here, a stronger change in the internal energy of the Si cluster is observed as it transforms into the silicon film than in the case of the Ag(001) substrate.

A significant distinction between the formation mechanisms of the

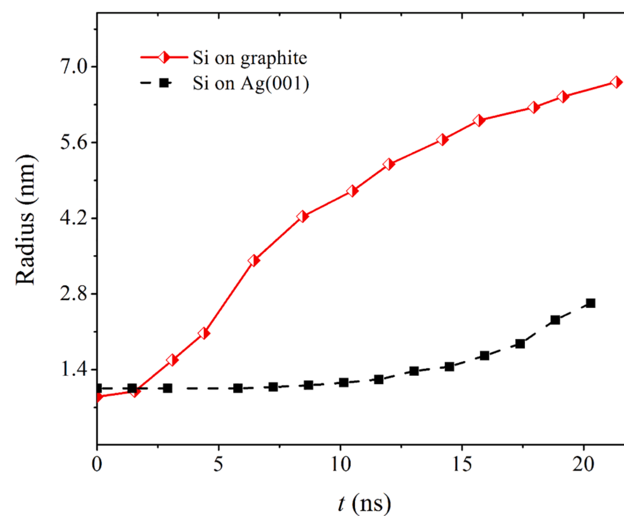

Fig. 9. Average radius of clusters formed on the surfaces of Ag(001) (black curve) and graphite (red curve) versus time. (For interpretation of the references to colour in this figure legend, the reader is referred to the web version of this article.)

silicon films on metallic and nonmetallic substrates may be primarily due to the difference in the energy of the silicon adhesion to the substrate. Fig. 8 shows the dependences of E_{ad} (t) for systems on the silver substrate (Fig. 8a) and on the graphite substrate (Fig. 8b). The top insets illustrate the average roughness value $< d >$ of the silicon films for two types of substrates, in addition, the characteristic appearance of the films at the initial moment of the stable cluster formation on the substrate is illustrated in the left part of Fig. 8 and at the end of the simulation it is presented in the right part of Fig. 8. The values of the adhesion energy at the current step depend on the total number of Si atoms in the system. It is known [35] that the adhesion energy between the silver surface and silicene is approximately 0.345 eV, which is the average value taken for substrate orientations (001), (111), (110). In the case of the Ag(001) substrate, the initially obtained value of the adhesion energy was 0.37 eV (Fig. 8a). Over time the value of $E_{ad}(t)$ decreased slightly and was about 0.3 eV, and by the time of 22.5 ns it reached the value of 0.345 eV.

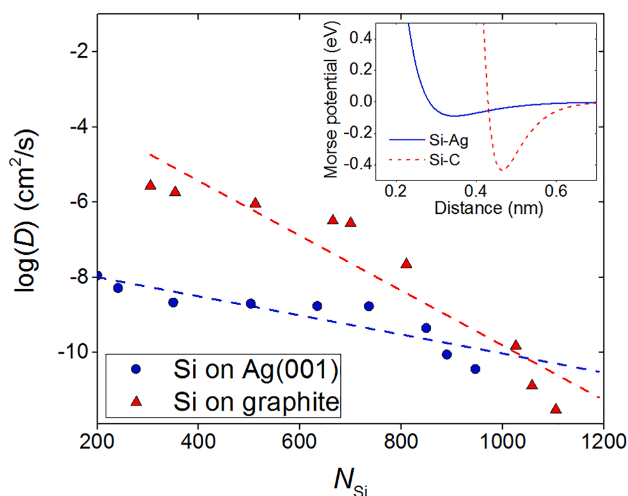

Fig. 10. Surface diffusion of silicon atoms on silver (in blue) and graphite (in red) surfaces, dashed lines show a linear approximation of the dependencies. The inset shows the structure of the Morse potential as a function of the equilibrium lattice parameter r^{o}_{ij},; Si-Ag interaction is presented in blue, Si-C interaction is presented in red. (For interpretation of the references to colour in this figure legend, the reader is referred to the web version of this article.)

After the silicon clusters are pulled together forming a single film, in some sites the second silicon layer formation begins. The formation of the second layer of Si atoms leads to a sharp decrease in the $E_{ad}(t)$ dependence. The maximum decrease in the adhesion energy is associated with the time instant of 27.9 ns, further, the value of $E_{ad}(t)$ fluctuates around 0.13 eV.

Fig. 8b demonstrates the time dependence of adhesion energy of the system on the graphite substrate. At the first stage (left part), the average value of E_{ad} is ≈ 0.174 eV, then it decreases to ≈ 0.051 eV. It should be noted, that in the case of the system on the silver substrate, the Si-film is more uniform in contrast to that on the graphite one. At the final stage of the simulation, the film on the silver substrate covers its entire surface, and the tendency towards three-dimensional growth is only outlined (the roughness $\langle d \rangle$ of the silicon film increases, but a uniform second layer of the film has not formed yet). In the case of graphite, the coating turns out to be more defective, however, the formation of the second silicon layer can be clearly traced.

Fig. 9 presents the change in the average radius of the formed Si-clusters over time. As follows from these dependencies the cluster growth on two different substrates are very different. The average cluster radius grows slowly on the metal surface (black line), but on the nonmetal surface (red line) the radius versus time function increases rapidly during 6 ns and further; the cluster radius increases gentler. In both cases, the change in the cluster size was traced as long as local Si formations could be observed on the substrate surface. It can be assumed, that the unequal nature of the surface diffusion of silicon atoms on two types of substrates is one of the reasons for the difference in cluster-growth dynamics.

The dependence of the surface diffusion on the number of Si-atoms in the system is provided in Fig. 10. The values are in the logarithmic scale, the blue dependence describes the system on silver, the red one describes the system on graphite. In the case of the silver substrate, the mobility of Si atoms at the initial moment of time turns out to be equal to 1.12×10^{-8} cm^2/s and to decrease gradually with time. A sharp decrease in log D values occurs at $N_{Si} = 840$. The silicon atoms on the graphite substrate have the higher surface diffusion of 2.72×10^{-6} cm^2/s at the initial stage. This is largely due to the lower value of the adhesion of the Si/graphite system. At the same time, the internal energy of the silicon film on the graphite substrate has lower (more negative) values than on the silver substrate. It can be noted, that the characteristic magnitude of the surface diffusion of nonmetallic particles on different surfaces

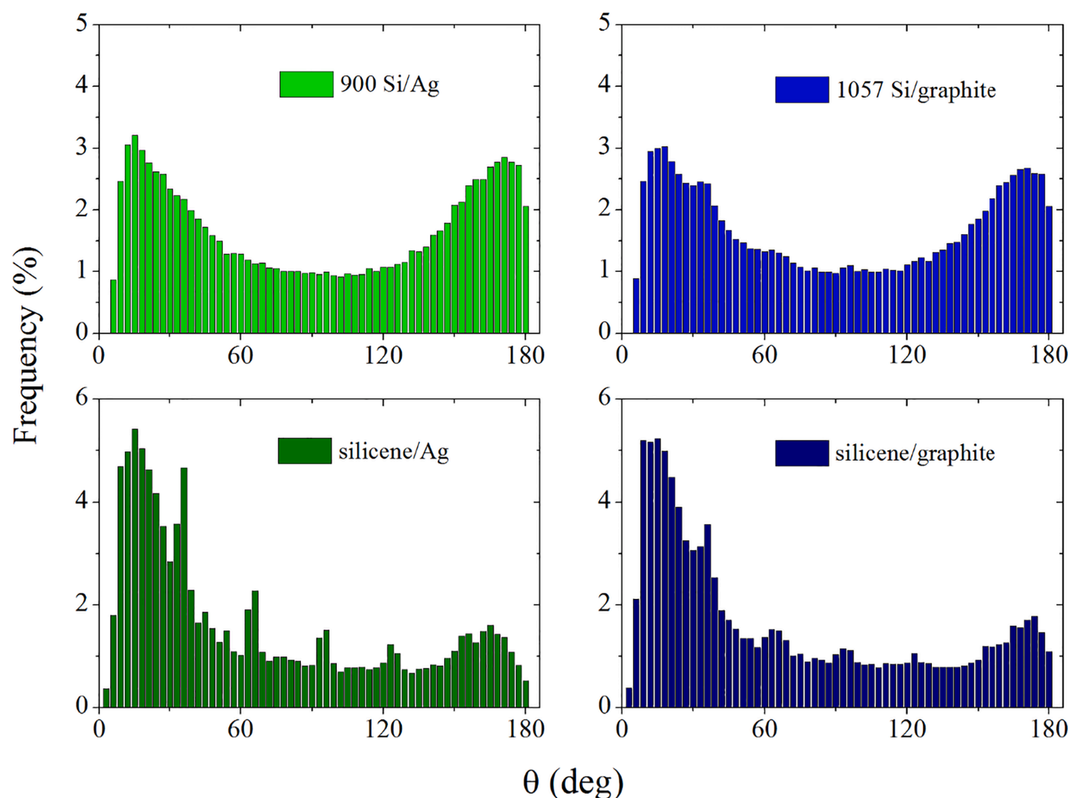

Fig. 11. Angular distributions of the nearest geometric neighbors for a single-layer silicon film deposited on Ag (001) and on a graphite substrate (the number in the legend shows the number of deposit Si atoms), and for silicene on the corresponding substrates.

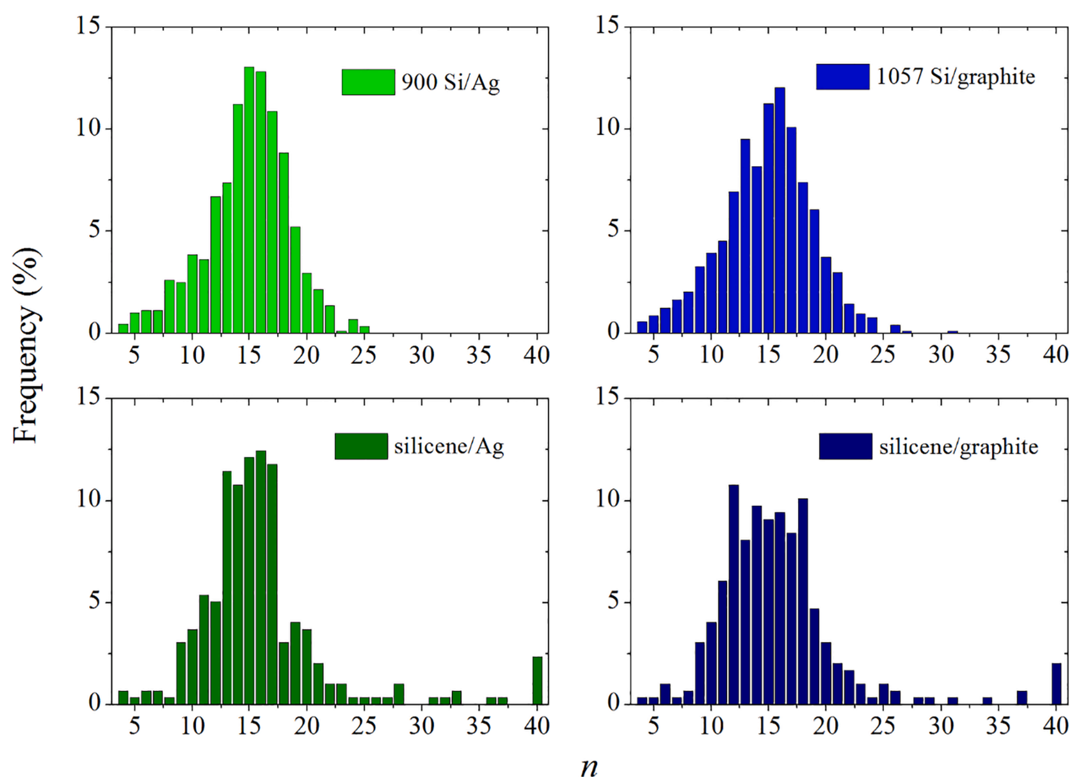

Fig. 12. Distribution of Voronoi polyhedra by the number of faces for a single-layer silicon film deposited on the Ag (0 0 1) and graphite substrates (the number in the legend shows the number of deposited Si atoms), and for silicene posted on the corresponding substrates.

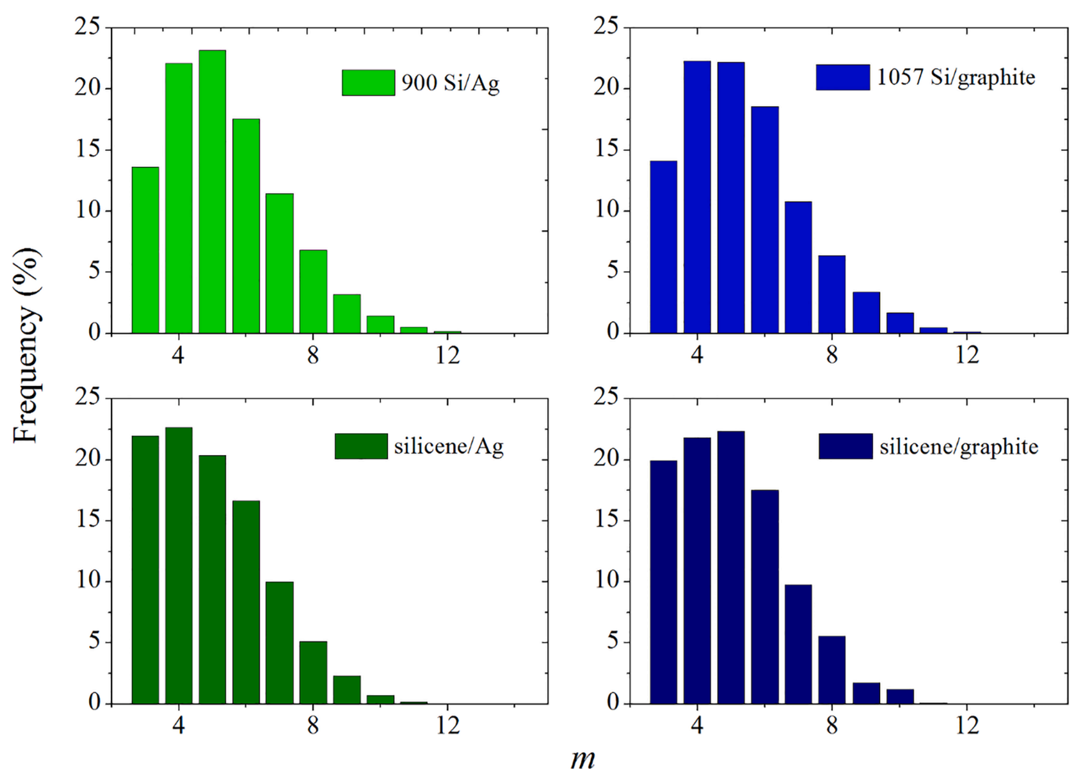

Fig. 13. Distribution of VP faces by the number of sides for a single-layer silicon film deposited on the Ag (0 0 1) and graphite substrates (the number in the legend shows the number of deposited Si atoms), and for silicene on the corresponding substrates.

obtained by various authors is in the range of 10^{-3}– 10^{-9} cm^2/s [37]. The inset in Fig. 10 shows the Morse potentials describing the Si-Ag and Si-C interactions. The Discussion section explains the effect of the nature of these interactions on the diffusion of Si atoms over the substrate surface.

When constructing the angular distribution of geometric neighbors, we considered the angles θ enclosed between the rays drawn from the VP

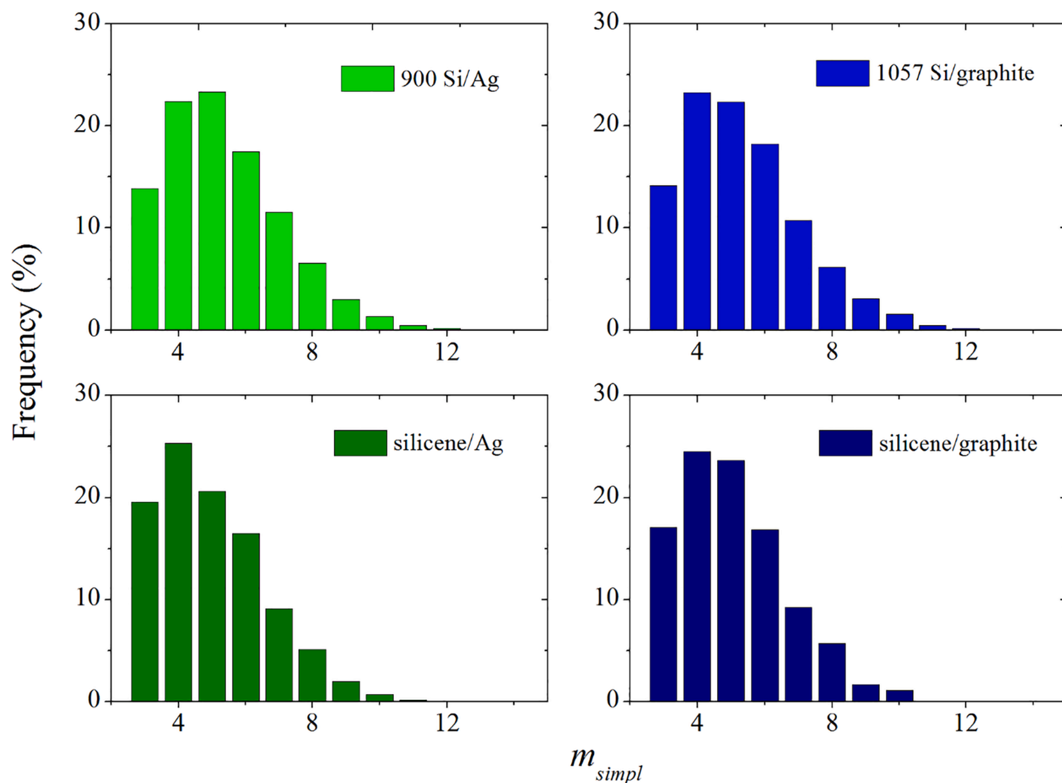

Fig. 14. Distribution of the faces of simplified polyhedrons by the number of sides for a single-layer silicon film deposited on the Ag (001) and graphite substrates (the number in the legend indicates the number of deposited Si atoms), and for silicene on the corresponding substrates.

center to the centers of neighboring atoms giving the VP faces. The calculated angular distributions (Fig. 11) show that there is a difference in the angular arrangement of Si atoms in the obtained single-layer films and in silicene, where acute angles in the vicinity of 15° are more strictly maintained. Such angles are due to the presence of buckles in silicene. Both for the deposited silicon film and for silicene, the VP distributions over the number of faces (n distributions) obtained using a graphite substrate are more symmetric and have lower standard deviations than the corresponding distributions related to the Ag(001) substrate (Fig. 12). The standard deviations for n distributions obtained for silicene are lower than those for the corresponding Si films by 2.1% (Ag (001) substrate) and 2.3% (graphite substrate). Silicon films obtained by the deposition on substrates have significantly lower vertical displacements of atoms than the height of silicene buckles, which increases when silicene is placed on the substrate. Due to the wide set of local bulges in the silicene on the substrate, the n distribution for the VPs constructed for it turns out to be elongated over a wide interval (up to n = 40).

The main difference between the distributions of the VPs faces by the number of sides (m distributions) for the obtained Si films against silicene on the corresponding substrates is the presence of a big number of triangular faces in m distributions of silicene (Fig. 13). Thus, in the case of the Ag (001) substrate, the m distributions in silicene have 37.9% more triangular faces, and using the graphite substrate for silicene, such faces are 26.6% larger than those for the obtained Si film. Triangular faces generally have a small area and belong to more distant geometric neighbors. When constructing simplified polyhedra (taking into account only straight geometric neighbors), small geometric elements are excluded [38]. The distribution of the faces of such polyhedra by the number of sides shows a reduction in the proportion of triangular faces (Fig. 14). Moreover, the difference in the number of triangular faces in simplified polyhedrons for silicene and the deposited Si film decreased to 29.4% and 17.1% when the Ag (001) and graphite substrates were used, respectively. In the case of the graphite substrate, the ratio

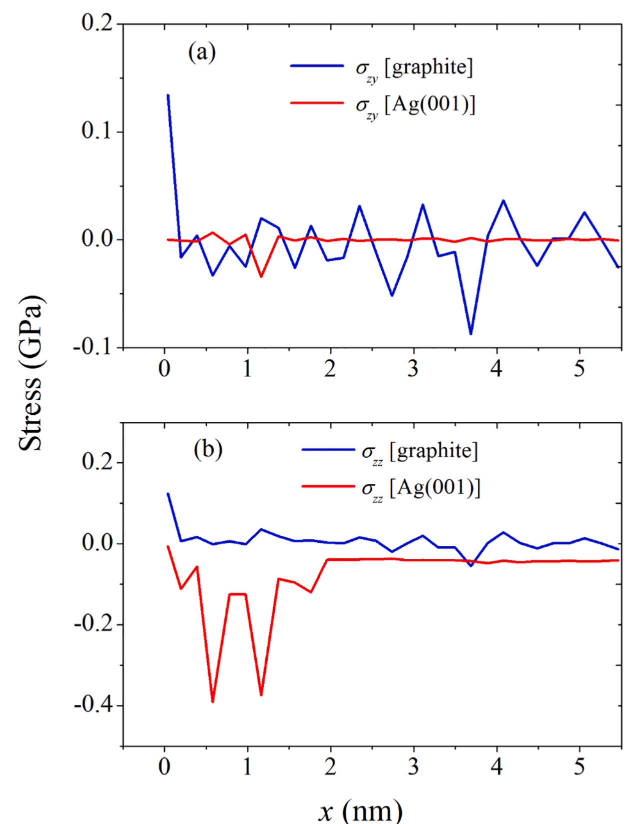

Fig. 15. Distribution of (a) lateral σ_{zy} and (b) normal σ_{zz} stresses for the silicon film obtained on the graphite and Ag (001) substrates along the 0x direction, when the elementary areas are elongated along the 0y direction.

between other types of faces for the deposited Si film and silicene is more accurate than in the case of the Ag (001) substrate. The same conclusion can be drawn when considering the corresponding distributions constructed for simplified polyhedra. Thus, the Si film deposited on the graphite substrate corresponds more to the silicene structure than the film deposited on the Ag (001) substrate.

The strongest local stresses in silicon films obtained on the graphite and silver substrates are compared in Fig. 15. Normal local stresses σ_{zz} for the Si film deposited on the Ag (001) substrate can reach the values that are almost 4 times higher than the corresponding stresses that exist in a similar film grown on the graphite surface. At the same time, the lateral local stresses σ_{zy} turn out to be much more significant when the film is located on the graphite substrate. Note that the amplitudes of the fluctuations of the normal stress σ_{zz} in the film on the silver substrate are much larger than the corresponding characteristics of the lateral stress σ_{zy}. However, for the film on the graphite substrate, the values of these characteristics are comparable.

4. Discussion

In this work, a molecular dynamic model describing the formation process of the silicon film on two types of substrates was developed. It was found that the difference in the substrate material affects the surface diffusion of silicon and, as a consequence, leads to the formation of various two-dimensional structures on silver and graphite substrates. We applied a simplified molten salt electrodeposition model to obtain silicon films of the monoatomic thickness. The model shows the possibility of adjusting the thickness of the resulting film, since the process implies mainly a layer deposition, especially in the case of the silver substrate.

The stronger diffusion of silicon over the surface of the graphite substrate as compared to the Ag (001) substrate is explained by the nature of the “Si-substrate” interaction. The inset in Fig. 10 shows the Si-C and Si-Ag interaction potentials used. Under the action of an electric field, Si^{4+} ions move downward and collide with the substrate. This interaction with the substrate is characterized by a repulsive branch of the corresponding Morse potential. The steeper repulsive branch of the Si-C potential provides more intense movement of Si atoms over the graphite surface. The deposition of the Si^{4+} ion on the Ag (001) surface has a gentler character in accordance with the shape of the repulsive branch of the Si-Ag potential. A moving Si atom interacts more often with the substrate atoms (gaining greater acceleration) in the case when the substrate is graphite rather than silver. This is due to a larger number of C atoms than Ag atoms per one and the same substrate area. In addition, the size of the C atoms is smaller than the size of the Ag atoms, i.e. the carbon substrate is smoother. All of these contribute to a faster diffusion of Si atoms over the surface of the graphite substrate. The substantially deeper potential well of the Si-C potential creates conditions for the condensation, i.e. the formation of one large cluster on the surface of the graphite substrate.

The correlation between the values of Si surface diffusion and the Si-substrate adhesion energy is established. Specifically, the lower value of E_{ad} (in the case of the graphite substrate) contributes to the higher mobility of silicon atoms. Additionally, the difference in the adhesion energy affects the growth mechanisms of clusters: several growth centers of the silicon film were found on the metallic substrate, and one active growth center was observed on graphite. The difference in the mechanisms of film growth neutralizes the high mobility of Si atoms on the graphite surface and leads to almost the same deposition time of the film as in the case of deposition on a silver substrate.

At the temperature of 1000 K in the presence of a liquid electrolyte, the packing of Si atoms in the growing silicon film does not undergo significant changes as the coating of the electrode surface approaches to the end. Thus, a fairly stable angular distribution of the nearest geometrical neighbors is established in the growing Si films on the Ag (001) and graphite substrates even when the filling of the electrode

Table 3
Mean value and standard deviation of lateral σ_{zy} and normal σ_{zz} stress distributions in the silicon film on the silver and graphite substrates.

Substrate	Ag(001)		Graphite	
Stress	Mean	Standard Deviation	Mean	Standard Deviation
σ_{zy}, MPa	−0.7958	78.54	−2.26	36.96
σ_{zz}, MPa	6.78	89.55	6.87	27.78

surface with silicon reaches 70–80%. The same level of filling the electrode surface with silicon provides 7–8% retention of the standard deviation for n distributions, while the variation of the standard deviation for the m distributions does not exceed 3% using both the Ag (001) and graphite substrates. It is very likely that the structural relaxation of the silicon film will continue after cooling to room temperature due to the appearance of stresses caused by different coefficients of thermal expansion of the substrate and the film.

It is of interest to obtain more detailed characteristics of the stress distributions shown in Fig. 15. The average values of the calculated stresses and the standard deviations obtained from them are shown in Table 3.

The absolute value of the average lateral stress σ_{zy} in the silicon film on the graphite substrate is higher than the corresponding characteristic of the film on the silver substrate. At the same time, the average normal stresses σ_{zz} for the obtained Si film on silver and graphite substrates are approximately the same. The standard deviations for both stresses related to the Si film on the Ag (001) substrate are significantly higher than the corresponding characteristics obtained for a film on the graphite substrate. Large values of the standard deviation show strong variability in the statistic. Consequently, a silicon film obtained on graphite is characterized by more uniform values of local stresses σ_{zy} and σ_{zz} distributed over the entire film area than that is the case for the film grown on the Ag (001) substrate. The highest local normal stress σ_{zz} that appears in the silicon film on the Ag (001) substrate is 32 times lower than the tensile strength of free-standing silicene (12.5 GPa) [39].

The silicon films obtained in this work both on the silver and graphite substrates contained five-links rings formed by Si atoms. As a rule, the rings triplets were combined to form a common vertex between them. Combinations of three five-link rings were observed on both types of substrates, but they are more common for silver substrates. We earlier reported that the analogous associations appeared when monovacancies were created in silicene [40]. It is known, that regular pentagons cannot continuously and densely cover large surfaces. However, if the coating is made of pentagons, not lying on the same plane, then the pentagons can be densely (without voids and overlaps) packed over a large area, e.g. this is how the model of pentasilicene, which retains many properties of ordinary silicene is formed by hexagonal honeycombs, was created [41].

It was found that, during the electrodeposition of silicon onto the graphite substrate, regions of hexagons are formed with Si atoms at their vertices. Each of these areas has a winding boundary. Boundaries could include five- and four-link polyhedrons formed by Si atoms. Similar structures, only on a larger scale, were obtained in a physical experiment on the carbon substrate, more precisely, on highly oriented pyrolytic graphite (HOPG) by deposition under ultrahigh vacuum conditions [42]. In some regions of HOPG small 3D clusters were found. According to the scanning tunneling microscopy evidence, silicene on the HOPG substrate has a very insignificant deformation (0.05 nm). The obtained silicene monolayer on the HOPG surface is stable both at room temperature and at 350 °C. In present work, we also found a tendency towards the formation of 3D structures during the electrolytic deposition of silicon on the graphite substrate. Silicene on the graphite substrate is a much less expensive option for electronics and electrochemical devices than silicene on the silver substrate [43]. At the same time, there are fundamental difficulties in the implementation of silicene sheets on silver substrates as electrodes of a lithium-ion battery [44].

The results of this work bring a certain understanding to the process

of silicon electrodeposition on silver and graphite substrates. It is shown that the perfect crystal structure of a metallic or non-metallic substrate cannot guarantee the formation of a single-layer silicon structure of the "honeycomb" type. It is quite possible that one-stage process of electrodeposition is not sufficient to obtain such structure. It is possible that the subsequent thermal annealing will relieve the mechanical stress of the film and bring its structure closer to that of silicene. It is more difficult to obtain a strictly two-dimensional film on a graphite substrate than on an Ag (0 0 1) substrate. This is due to the weak interaction between the silicon film and the graphite substrate. In this case, in the absence of filling the entire substrate with a perfect hexagonal silicon structure associated with sp^2 hybridization, the tendency to sp^3 hybridization characteristic of bulk silicon increases. As a result, islands of new layers begin to form on the silicon film, which prevents the formation of a strictly single-layer coating. It is possible that with a decrease in the current density during the electrolysis may improve the quality of a single-layer silicon film on a graphite substrate.

The Ag (0 0 1) substrate provides a stable layer-by-layer growth of a silicon film during the electrolytic production. This is facilitated by the relatively low and not rapidly changing over time value of the self-diffusion coefficient of silicon ions. At present, it is on this substrate that silicene is most often obtained by the epitaxy in high vacuum. The question of whether the Dirac cone is retained in the electronic structure of silicene is still debatable when it is placed on a silver substrate [35]. The process of electrolytic production of thin silicon films on a graphite substrate requires careful optimization, because of the high and rapidly changing values of the self-diffusion coefficient of Si^{4+} ions. In addition, the tendency of deposited Si atoms towards sp^3 hybridization, which leads to disruption of layer-by-layer film growth [45,46], is manifested here more than in the case of adsorption on metallic substrates.

The electrolytic method is used to obtain pure silicon films [5]. Films of a more complex composition, for example, silicon nitride films, are produced by a chemical method using precursors [47]. It was shown that in the presence of van der Waals interactions between the film and the substrate, an impurity at the growth front of the film can favor a flat morphology [48]. For example, the addition of Cu to Ag during the entire film growth period leads to the formation of a smoother film surface on a SiO_2 substrate.

From the point of view of using thin silicon films, in particular, silicene, in microelectronics, their production on a carbon substrate is more promising than the deposition of silicene on a silver substrate [49]. The fact is that the use of silicene in devices such as a field effect transistor requires it to be placed on an insulating substrate. Until now, the transfer of silicene to an insulating substrate has not been carried out. However, it is obvious that such transfer without destruction of silicene is easier to carry out from a graphite substrate than from a metallic one, since the adhesion force of silicene with graphite is significantly less.

It is known that solar cell efficiency is very sensitive to even low-level recombinations. This requires high purity of the active material that converts solar energy into electrical energy. Lowering production costs and improving the efficiency of silicon solar cells are becoming critical to increase the share of photovoltaic electricity in the current energy mix and this demand will steadily grow in the future. Continuous improvement of silicon solar cells brings their performance closer to the theoretical efficiency limit. However, the gap between the achieved and theoretical possibilities still exists.

5. Conclusions

The production of thin silicon films by the electrolytic method can solve the problem of industrial production of solar silicon. In this work, we have shown the fundamental possibility of producing ultrathin films of pure silicon by this method. Two substrates for deposition of thin silicon layers are considered. Both silver and graphite substrates are found to be compatible with this process. A graphite substrate is a cheaper base, but a layered 2D silicon structure is more easily formed on a silver substrate. In addition, the adhesion energy of the continuous silicon film formed on the silver substrate is 2.5 times higher than that of the corresponding Si film on the graphite substrate. This provides the "Si-film / Ag-substrate" product greater strength in service. However, in this case, the unique properties of silicene, which determine its applicability in nanoelectronics, nanophotonics, and spintronics, can be largely deteriorated. An ideal single crystal layer was not obtained on any substrates used. The study of the detailed structure of silicon films obtained by the model electrodeposition showed that the films had a highly distorted hexagonal structure, where five and four-link formations were present in their horizontal projection, together with hexagons. In addition to these features, the films differed from the "honeycomb" structure characteristic of free-standing silicene by lower local buckles. The silicon films obtained on the graphite substrate were found to have a structure closer to silicene than those obtained on the Ag (0 0 1) substrate. The silicon films synthesized by electrolytic deposition had a low mechanical stress, which was more uniformly distributed if the film was deposited on the graphite substrate. The defects created in the silicon layer of monoatomic thickness should not lead to recombination. Unfortunately, the limited time scale of MD simulation did not allow us to solve the problem of stability of the obtained defect structures. Obviously, a solution to this issue can be expected when conducting natural experiments.

Progress in the field of electrolytic production of thin films of high-purity silicon can be achieved by combining efforts and approaches in the fields of physics, chemistry, materials science, engineering solutions and economics.

CRediT authorship contribution statement

Ksenia A. Ivanichkina: Conceptualization, Methodology, Software, Writing - original draft, Formal analysis. **Alexander Y. Galashev:** Conceptualization, Writing - review & editing, Formal analysis, Project administration. **Andrey V. Isakov:** Conceptualization, Resources.

Declaration of Competing Interest

The authors declare that they have no known competing financial interests or personal relationships that could have appeared to influence the work reported in this paper.

Acknowledgements

This research did not receive any specific grant from funding agencies in the public, commercial, or not-for-profit sectors.

Appendix A

The total energy E_{tot} of Ag atoms in a silver support is given by the EAM potential as [19]

$$E_{tot} = \sum_i F(\langle\rho\rangle_i) + \frac{1}{2}\sum_{i\neq j} \text{É¸}(r_{ij}) \quad \text{(B.1)}$$

Table A1
Parameters of the Tersoff potential for carbon.

Parameters	Carbon
A (eV)	1393.6
B (eV)	346.74
λ_1 (nm)$^{-1}$	34.879
λ_2 (nm)$^{-1}$	22.119
n	0.72751
c	$3.8049 \cdot 10^4$
d	4.384
$R^{(1)}$ (nm)	0.18
$R^{(2)}$ (nm)	0.23
β	$1.5724 \cdot 10^{-7}$
h	−0.57058

and

$$\langle \rho_i \rangle = \sum_j \rho(r_{ij}) \tag{B.2}$$

where F is an embedding to embed an atom i in the combined electron density $\langle \rho \rangle_i$, contributed by neighbouring atoms j by an amount $\rho(r_{ij})$, the pair potential function $\phi(r_{ij})$ shows the energy of bond ij which is due to the short-range electro-static interatomic interaction, and r_{ij} is the distance between an atom i and its neighbor j.

The main advantages of EAM potential are the simple form of potential and the fact that it is based on density functional theory (DFT). However, its embedded energy F and pair potential $\phi(r_{ij})$ are given in the form of spline functions which leads to some disadvantages for calculations [50]. Arrays of parameters $F_i(\rho_{h,i})$, $\rho_{h,i}$, $\phi_{ij}(R_{ij})$ specify this potential.

The interaction between C atoms and graphite sheets was described by the Tersoff potential [17]

$$V_{ij} = f_C(r_{ij})\left[A\cdot\exp\left(-\lambda^{(1)} r_{ij}\right) - Bb_{ij}\cdot\exp\left(-\lambda^{(2)} r_{ij}\right)\right], \tag{B.3}$$

$$f_C(r_{ij}) = \begin{cases} 1, & r_{ij} < R^{(1)} \\ \frac{1}{2} + \frac{1}{2}\cos\left[\pi\left(r_{ij} - R^{(1)}\right)/\left(R^{(1)} - R^{(2)}\right)\right] & R^{(1)} < r_{ij} < R^{(2)} \\ 0, & r_{ij} > R^{(2)} \end{cases} \tag{B.4}$$

where b_{ij} is the multi-particle bond-order parameter describing the manner of the bond-formation energy (attractive part V_{ij}) is created at the local atomic arrangement because of the presence of the neighboring atoms. $R^{(1)}$ and $R^{(2)}$ are the parameters of the potential cutoff. The potential energy is a multi-particle function of atomic positions i, j and k, which are determined by parameters

$$b_{ij} = \left(1 + \beta^n \xi_{ij}^n\right)^{-1/2n}, \tag{B.5}$$

$$\xi_{ij}^n = \sum_{k \neq i,j} f_C(r_{ij}) g(\theta_{ijk}), \tag{B.6}$$

$$g(\theta_{ijk}) = 1 + \frac{c^2}{d^2} - \frac{c^2}{\left[d^2 + (h - \cos\theta_{ijk})^2\right]}, \tag{B.7}$$

where ξ_{ij} is the effective coordination number, $g(\theta_{ijk})$ is the function of the angle between r_{ij} and r_{ik}, which stabilizes the tetrahedral structure.

Table A1 shows the parameters of the Tersoff potential used to describe the interactions in graphite.

Appendix B. Supplementary material

Supplementary data to this article can be found online at https://doi.org/10.1016/j.apsusc.2021.149959.

References

[1] L.C. Andreani, A. Bozzola, P. Kowalczewski, M. Liscidini, L. Redorici, Silcon solar cell: towards the efficiency limits, Adv. Phys.: X 4 (2019) 1548305, https://doi.org/10.1080/23746149.2018.1548305.

[2] W. Xiao, D. Wang, The electrochemical reduction processes of solid compounds in high temperature molten salts, Chem. Soc. Rev. 43 (2014) 3215–3228, https://doi.org/10.1039/C3CS60327J.

[3] K. Yasuda, K. Maeda, T. Nohira, R. Hagiwara, T. Homma, Silicon electrodeposition in water-soluble KF-KCl molten salt: optimization f electrolysis conditions at 923 K, J. Electrochem. Soc. 163 (2016) D95, https://doi.org/10.1149/2.0791603jes.

[4] A.O. Khudorozhkova, A.V. Isakov, A.A. Red'kin, Y.P. Zaikov, Zaikov, Liquidus temperatures of KF-KCl-KI melts, Russian Metallurgy (Metally) 2019 (8) (2019) 830–834, https://doi.org/10.1134/S0036029519080081.

[5] A.V. Isakov, A.P. Apisarov, A.O. Khudorozhkova, M.V. Laptev, Y.P. Zaikov, Electrodeposition of silicon onto copper substrate from KF-KCl-KI-K_2SiF_6 melt, J. Phys. Conf. Series 1134 (2018) 012021, https://doi.org/10.1088/1742-6596/1134/1/012021.

[6] X. Zou, L.i. Ji, X. Yang, T. Lim, E.T. Yu, A.J. Bard, Electrochemical formation of a p-n junction on thin film silicon deposited in molten salt, J. Am. Chem. Soc. 139 (45) (2017) 16060–16063, https://doi.org/10.1021/jacs.7b0909010.1021/jacs.7b09090.s001.

[7] J. Ustarroz, X. Ke, A. Hubin, S. Bals, H. Terryn, New insights into the early stages of nanoparticle electrodeposition, J. Phys. Chem. C 116 (3) (2012) 2322–2329, https://doi.org/10.1021/jp210276z.
[8] A.Y. Galashev, K.A. Ivanichkina, K.P. Katin, M.M. Maslov, Computer test of a modified silicene/graphite anode for lithium-ion batteries, ACS Omega 5 (22) (2020) 13207–13218, https://doi.org/10.1021/acsomega.0c0124010.1021/acsomega.0c01240.s001.
[9] H.O. Nam, A. Bengtson, K. Vörtler, S. Saha, R. Sakidja, D. Morgan, First-principle molecular dynamics modeling of the molten fluoride salt with Cr solute, J. Nucl. Mater. 449 (2014) 148–157, https://doi.org/10.1016/j.jnucmat.2014.03.014.
[10] A.E. Gheribi, P. Chartrand, Thermal conductivity of molten salt mixtures: Theoretical model supported by equilibrium molecular dynamics simulations, J. Chem. Phys. 144 (8) (2016) 084506, https://doi.org/10.1063/1.4942197.
[11] X. Wang, C. Chen, K. Binder, U. Kuhn, U. Pöschl, H. Su, Y. Cheng, Molecular dynamics simulation of the surface tension of aqueous sodium chloride: from dilute to highly supersaturated solutions and molten salt, Atmos. Chem. Phys. 18 (23) (2018) 17077–17086, https://doi.org/10.5194/acp-18-17077-201810.5194/acp-18-17077-2018-supplement.
[12] G. Le Lay, B. Aufray, C. Léandri, H. Oughaddou, J.-P. Biberian, P. De Padova, M. E. Dávila, B. Ealet, A. Kara, Physics and chemistry of silicene nano-ribbons, Appl. Surf. Sci. 256 (2) (2009) 524–529, https://doi.org/10.1016/j.apsusc.2009.07.114.
[13] B. Feng, Z. Ding, S. Meng, Y. Yao, X. He, P. Cheng, L. Chen, K. Wu, Evidence of silicene in honeycomb structures of silicon on Ag(111), Nano Lett. 12 (7) (2012) 3507–3511, https://doi.org/10.1021/nl301047g.
[14] P. Scheier, B. Marsen, M. Lonfat, W.-D. Schneider, K. Sattler, Growth of silicon nanostructures on graphite, Surf. Scie. 458 (1-3) (2000) 113–122, https://doi.org/10.1016/S0039-6028(00)00426-X.
[15] B. Feng, Z. Ding, S. Meng, Y. Yao, X. He, P. Cheng, L. Chen, K. Wu, Evidence of silicene honeycomb structures of silicon on Ag(111), Nano Lett. 12 (2012) 3507–3511, https://doi.org/10.1021/nl301047g.
[16] S.M. Foiles, M.I. Baskes, M.S. Daw, Embedded-atom-methode functions for the fcc metals Cu, Ag, Au, Ni, Pd, Pt and their alloys, Phys. Rev. B 33 (1986) 7983, https://doi.org/10.1103/PhysRevB.33.7983.
[17] J. Tersoff, Modelng solid-state chemistry: Interatomic potentials for multicomponent systems, Phys. Rev. B: Condens. Matter Mater. Phys. 39 (1989) 5566, https://doi.org/10.1103/PhysRevB.39.5566.
[18] J. Zhao, P.J Culligan, Y. Qiao, Q. Zhou, Y. Li, M. Tak, T. Park, X. Chen, Electrolyte solution transport in electropolar nanotubes, J.Phys.: Condens. Mater. 22 (2010) 315301 (12). https://doi.org/10.1088/0953-8984/22/31/315301.
[19] M. Ferrario, G. Ciccotti, E. Spohr, T. Cartailler, P. Turq, Solubility of KF in water by molecular dynamics using the Kirkwood integration method, J. Chem. Phys. 117 (10) (2002) 4947–4953, https://doi.org/10.1063/1.1498820.
[20] J.M. Hu, J.P. Zhai, F.M. Wu, Z.K. Tang, Molecular dynamics study of the structures and dynamics of the iodine molecules confined in $AlPO_4$-11 crystals, J. Phys. Chem. 114 (49) (2010) 16481–16486, https://doi.org/10.1021/jp1076615.
[21] H. Loulijat, H. Zerradi, A. Dezairi, S. Ouaskit, S. Mizani, F. Rhayt, Effect of Morse potential as model of solid-solid inter-atomic interaction on the thermal conductivity of nanofluids, Adv. Powder. Tech. 26 (1) (2015) 180–187, https://doi.org/10.1016/j.apt.2014.09.006.
[22] R. Yu, P. Zhai, G. Li, L. Liu, Molecular dynamics simulation of the mechanical properties of single-crystal bulk Mg_2Si, J. Electron. Mater. 41 (6) (2012) 1465–1469, https://doi.org/10.1007/s11664-012-1916-x.
[23] K. Mylvaganam, L.C. Zhang, Effect of oxygen penetration in silicon due to nano-indentation, Nanotechnology. 13 (2002) 623–626, 10.0957-4484/02/050623+04 $30.00.
[24] A.Y. Galashev, K.P. Katin, M.M. Maslov, Morse parameters for the interaction of metals with graphene and silicene, Phys. Lett. A. 383 (2-3) (2019) 252–258, https://doi.org/10.1016/j.physleta.2018.10.025.
[25] L. Grippo, S. Lucidi, A globally convergent version of the Polak-Ribier conjugate gradient methode, Math. Program. 78 (1997) 375–391, https://doi.org/10.1007/BF02614362.
[26] A. Khudorozhkova, A. Isakov, A. Apisarov, A. Redkin, Y. Zaikov, Liquidus temperature and electrical comductivity of the KF-KCl-KI system containing K_2SiF_6, J. Chem. Eng. Data 65 (2020) 2505–2511, https://doi.org/10.1021/acs.jced.9b01161.
[27] M.V. Laptev, A.V. Isakov, O.V. Grishenkova, A.S. Vorob'ev, A.O. Khudorozhkova, L.A. Akashev, Y.P. Zaikov, Electrodeposition of thin silicon films from the KF-KCl-KI-K_2SiF_6 melt, J. Electrochem. Soc. 167 (2020) 04206, https://doi.org/10.1149/1945-7111/ab7aec.
[28] K. Maeda, K. Yasuda, T. Nohira, R. Hagiwara, T. Homma, Silicon electrodeposition in water-soluble KF-KCl molten salt: Investigations on the reduction of Si(IV) ions, J. Electrochem. Soc. 162 (9) (2015) D444–D448, https://doi.org/10.1149/2.0441509jes.
[29] J.L. Finney, A procedure for the construction of Voronoi polyhedra, J. Comput. Phys. 32 (1) (1979) 137–143, https://doi.org/10.1016/0021-9991(79)90146-3.
[30] A.E. Galashev, V.P. Skripov, Investigation on the disordering of the argon hexagonal closed packed (HCP) crystals by the method of statistical geometry, J. Struct. Chem. 25 (1984) 734–740, https://doi.org/10.1007/BF00747917.
[31] A.E. Galashev, K.A. Ivanichkina, Computational study of the properties of silicon thin films on graphite, Rus. J. Phys. Chem. A 91 (12) (2017) 2448–2452, https://doi.org/10.1134/S003602441712007X.
[32] A.N. Novruzov, O.R. Rakhmanova, O.A. Novruzova, A.E. Galashev, The structure of water clusters interacting with gaseous acetylene, Rus. J. Phys. Chem. B 2 (2008) 115–122, https://doi.org/10.1134/S199079310801017X.
[33] K.J. Naidoo, M.M. Kuttel, Water structure about the dimer and hexamer repeat units of amylose from molecular dynamics computer simulations, J. Comput. Chem. 22 (2001) 445–456, https://doi.org/10.1002/1096-987X(200103)22:4<445::AID-JCC1015>3.0.CO;2-P.
[34] A.Y. Galashev, K.A. Ivanichkina, Computer test of a new silicene anode for lithium-ion battery, ChemElectroChem 6 (2019) 1525–1535, https://doi.org/10.1002/celc.201900119.
[35] J. Deng, J.Z. Liu, N.V. Medhekar, Enhanced lithium adsorption and diffusion on silicene nanoribbons, RSC Adv. 3 (2013) 20338–20344, https://doi.org/10.1039/C3RA43326A.
[36] H. Liu, J. Gao, J. Zhao, Silicene on substrates: interaction mechanism and growth behavior, J. Phys.: Conf. Ser. 491 (2014) 012007, https://doi.org/10.1088/1742-6596/491/1/012007.
[37] J.V. Barth, Transport of adsorbates at metal surfaces: from thermal migration to hot precursors, Surf. Sci. Rep. 40 (2000) 75–149, https://doi.org/10.1016/S0167-5729(00)00002-9.
[38] A.E. Galashev, Structure of water clusters with captured methane molecules, Rus. J. Phys. Chem. B 8 (6) (2014) 793–800, https://doi.org/10.1134/S1990793114110049.
[39] Q.-X. Pei, Z.-D. Sha, Y.-Y. Zhang, Y.-W. Zhang, Effects of temperature and strain rate on the mechanical properties of silicene, J. Appl. Phys. 115 (2) (2014) 023519, https://doi.org/10.1063/1.4861736.
[40] A.E. Galashev, K.A. Ivanichkina, Numerical simulation of the structure and mechanical properties of silicene layers on graphite during the lithium ion motion, Phys. Solid State 61 (2) (2019) 233–243, https://doi.org/10.1134/S1063783419020136.
[41] D. Wu, S. Wang, S. Zhang, Y. Liu, Y. Ding, B. Yang, H. Chen, Stabilization of two-dimensional penta-silicene for flexible lithium-ion battery via surface chemistry reconfiguration, Phys. Chem. Chem. Phys. 21 (2019) 1029–1037, https://doi.org/10.1039/c8cp05008b.
[42] M. Houssa, A. Dimoulas, A. Molle, Silicene: a review of recent of experimental and theoretical investigation, J. Phys.: Condens. Matter. 27 (2015), 253002, https://doi.org/10.1088/0953-8984/27/25/253002.
[43] A.E. Galashev, K.A. Ivanichkina, A.S. Vorob'ev, O.R. Rakhmanova, Structure and stability of defective silicene on Ag(001) and Ag(111) substrates: a computer experiment, Phys. Solid State. 59 (6) (2017) 1242–1252, https://doi.org/10.1134/S1063783417060087.
[44] A.Y. Galashev, K.A. Ivanichkina, Computer study of atomic mechanisms of intercalation/deintercalation of Li ions in a silicene anode on an Ag(111), J. Electrochem. Soc. 165 (2018) A1788–A1796, https://doi.org/10.1149/2.0751809jes.
[45] A.Y. Galashev, K.A. Ivanichkina, Silicene anodes for lithium-ion batteries on metal substrates, J. Electrochem. Soc. 167 (5) (2020) 050510, https://doi.org/10.1149/1945-7111/ab717a.
[46] A.Y. Galashev, O.R. Rakhmanova, K.A. Ivanichkina, Graphene and graphite supports for silicene stabilization: a computer study, J. Struct. Chem. 59 (2018) 877–883, https://doi.org/10.1134/S0022476618040194.
[47] T.R. Mayangsari, L.L. Yusup, R. Hidayat, T. Chowdhury, Y.-K. Kwon, W.-J. Lee, Reactivity of different nitriding agents with chlorine-terminated surface during atomic layer deposition of silicon nitride, Appl. Surf. Sci. 535 (2021) 147727, https://doi.org/10.1016/j.apsusc.2020.147727.
[48] A. Jamnig, N. Pliatsikas, G. Abadias, K. Sarakinos, On the effect of copper as wetting agent during growth of thin silver films on silicon dioxide substrates, Appl. Surf. Sci. 538 (2021) 148056, https://doi.org/10.1016/j.apsusc.2020.148056.
[49] A.Y. Galashev, A.S. Vorobev, Electronic and mechanical properties of silicene after nuclear transmutation doping with phosphorous, J. Mater. Sci. 55 (2020) 11367–11381, https://doi.org/10.1007/s10853-020-04860-8.
[50] S.M. Rassoulinejad-Mousavi, Y. Zhang, Interatomic potentials transferability for molecular simulations: a comparative study for platinum, gold and silver, Sci. Rep. 8 (2018) 2424, https://doi.org/10.1038/s41598-018-20375-4.